Interlayer charge transfer in ReS_{2}/WS_{2} van der Waals heterostructures

Peymon Zereshki, Peng Yao, Dawei He, Yongsheng Wang, and Hui Zhao

Phys. Rev. B **99**, 195438 — Published 21 May 2019

DOI: 10.1103/PhysRevB.99.195438

Interlayer Charge Transfer in ReS_2/WS_2 van der Waals Heterostructures

Peymon Zereshki,[1] Peng Yao,[2] Dawei He,[2] Yongsheng Wang,[2,*] and Hui Zhao[1,†]

[1]*Department of Physics and Astronomy, The University of Kansas, Lawrence, Kansas 66045, United States*
[2]*Key Laboratory of Luminescence and Optical Information, Ministry of Education, Institute of Optoelectronic Technology, Beijing Jiaotong University, Beijing 100044, China*

(Dated: May 9, 2019)

We observed ultrafast charge transfer between distorted-1T-ReS_2 with anisotropic in-plane electronic and optical properties and 2H-WS_2 that is in-plane isotropic. Heterostructures of monolayer ReS_2/monolayer WS_2 and bilayer ReS_2/monolayer WS_2 were fabricated by mechanical exfoliation and dry transfer techniques. Significant photoluminescence quenching of WS_2 in the heterostructures indicates efficient charge transfer. In femtosecond transient absorption measurements, it was found that holes injected in monolayer or bilayer ReS_2 transfer to WS_2 on a time scale shorter than time resolution of the measurement. This observation provides evidence that the holes are delocalized in bilayer ReS_2, revealing strong van der Waals interlayer couplings. These results also show that ReS_2 and WS_2 form type-II heterostructures with excellent charge transfer properties.

I. INTRODUCTION

Since 2010, two-dimensional (2D) transition metal dichalcogenides (TMDs) have been a focus of material research due to their interesting electronic, optical, and spin properties[1–3]. Although most initial efforts have been devoted to a few materials, namely MoS_2, WS_2, $MoSe_2$, and WSe_2[4], other members of the TMD family have gain significant momentum recently, especially those possessing different and complementary properties. Rhenium disulfide is such a member with several interesting properties. Unlike most TMDs with stable hexagonal phases, ReS_2 forms a distorted 1T structure with triclinic symmetry[5–7]. The lower lattice symmetry gives rise to in-plane anisotropic lattice, electronic, and optical properties, which have been confirmed by optical[8–12] and transport measurements[13–15]. In addition to the exfoliation method used in early studies, techniques to synthesize large-area and high-quality ReS_2 monolayer or thin films have been developed, such as epitaxy[16,17] and chemical vapor deposition[18,19]. Application of ReS_2 in various devices, such as transistors[20–24], logic gates[21], and polarization-sensitive photodetectors[20,22,25] have also been explored.

Despite of these progresses, some of the fundamental issues of this elusive material are still under debate. Most pressing ones include the nature of the lowest bandgap and the strength of the interlayer coupling. On the bandgap, early studies have indicated that bulk ReS_2 has a direct bandgap of about 1.5 eV at room temperature[5,26–29]. However, an indirect bandgap of 1.47 eV has been reported[30]. Low photoluminescence (PL) quantum yield generally observed in all thickness appear to suggest that ReS_2 is indirect semiconductor[31], while k-space photoemission microscopy revealed a direct bandgap in the bilayer (2L) ReS_2[32]. On the second issue, early experimental and first-principle studies have suggested that the interlayer coupling in ReS_2 is much weaker than other TMDs[5]. This suggests that the adjacent 1Ls in bulk ReS_2 are largely electronically decoupled with the electrons localized in each layers. The extremely weak van der Waals coupling in vertical ReS_2 nanowalls is recently utilized for high-current-density Li-ion batteries[33]. However, several evidences have been later reported that suggest rather strong interlayer coupling. First, optical absorption and PL measurements showed that the room-temperature optical bandgap evolves gradually from 1.47 eV in bulk to 1.61 eV in 1L[10]. Second, interlayer phonon modes were observed in Raman measurements, indicating that the ReS_2 layers are coupled and orderly stacked[34,35]. The interlayer force constants were about 55 - 90 % of those of multilayer MoS_2[36]. Third, photoemission microscopic measurements showed that the valence electrons in bulk ReS_2 are delocalized across the layers and the valence band dispersion evolves with the thickness[32]. In addition, qualitatively different charge transport characteristics between 1L and multilayers[37] appear to suggest thickness-dependent bandstructures.

Here we report direct evidence of electron interlayer delocalization in 2L ReS_2 by comparing charge transfer in 1L-ReS_2/1L-WS_2 and 2L-ReS_2/1L-WS_2 heterostructures fabricated by mechanical exfoliation and dry transfer. Interlayer charge transfer between 2D materials[38–44] plays a key role in forming 2D heterostructures with emergent properties. Therefore, study of charge transfer between ReS_2 and other TMDs is an important step towards introducing ReS_2 to the material library for constructing 2D heterostructures. Interestingly, recent studies have revealed that ReS_2 can form type-I band alignment with MoS_2[45], type-II band alignment with WSe_2[46], and type-III broken-gap alignment with black phosphorus[47], illustrating the flexibility of band alignment design ReS_2 can provide. However, despite of the recent progress on their growth[48] and device applications[46,49], the charge transfer process in ReS_2-based heterostructures is still yet to be studied. In this study by transient absorption and steady-state PL measurements, we found that holes optically injected in ReS_2 transfer to WS_2 on a sub-100 fs time scale, and the transfer from 2L ReS_2 appears to be even faster. This observation suggests that the holes in 2L ReS_2 are not localized in each ReS_2 layer, and thus provide direct evidence of electronic delocalization in this material. Furthermore, the ultrafast charge transfer between Re_2 and WS_2 is encouraging news for developing van der Waals heterostructures using ReS_2.

II. SAMPLE FABRICATION AND PHOTOLUMINESCENCE

Figure 1(a) shows the fabricated sample. First, a ReS_2 flake containing 1L and 2L regions was mechanically exfoliated on a polydimethylsiloxane (PDMS) substrate. Since the substrate (about 1 mm) is much thicker than the ReS_2 flake and is transparent, the optical contrast of the flake is proportional to its thickness[11,51–54]. By investigating a large number of thin flakes, we establish that the contrast of 1L is about 15.5%. Next, the selected ReS_2 flake was transferred to a Si/SiO_2 (90 nm) substrate. A 1L WS_2 fabricated and identified with the same procedure was then transferred on top of the ReS_2 flake such that it covers parts of both 1L and 2L ReS_2 regions as well as the substrate. Hence, the same sample contains heterostructure regions of 1L-ReS_2/1L-WS_2 and 2L-ReS_2/1L-WS_2, as well as a 1L WS_2 region. The sample was annealed for 4 hours at 200°C under 100 sccm of Ar gas environment with a pressure of 2 - 3 Torr. All measurement were done at room temperature with the sample under ambient conditions.

The expected band alignment of the 1L-ReS_2/1L-WS_2 heterostructure is shown in Figure 1(b). The values shown are adopted from a theoretical study[50]. The conduction band minimum (CBM) and the valence band maximum (VBM) are located in the ReS_2 and WS_2 layers, respectively. Such a type-II band alignment allow charge transfer, *i.e.* electron transfer from WS_2 to ReS_2 and hole transfer along the opposite direction. Since the offsets in the conduction and valence bands of 0.58 and 0.37 eV are much larger than the room-temperature lattice thermal energy of 0.025 eV, thermal excitation is unlikely to affect the direction of charge transfer. We note that although other theoretical works have yielded slightly different values of the band offsets, the

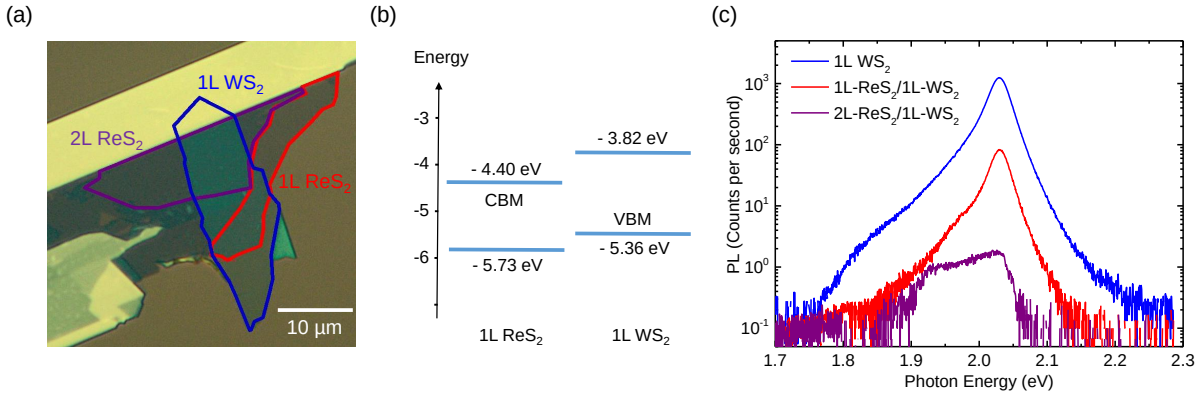

FIG. 1. (a) An optical microscopy image of the sample. (b) Band alignment of 1L-ReS_2/1L-WS_2 according to theory[50]. (c) PL of 1L WS_2 (blue), 1L-ReS_2/1L-WS_2 (red), and 2L-ReS_2/1L-WS_2 (purple).

type-II nature of the alignment has been consistently produced[32,45,55,56].

Figure 1(c) shows the PL spectra from regions of 1L WS_2 (blue), 1L-ReS_2/1L-WS_2 (red), and 2L-ReS_2/1L-WS_2 (purple), respectively. The measurement was performed with a 405-nm continuous-wave laser with a 200-nW power and a focused spot size of about 2 μm. The spectrum of 1L WS_2 peaks at 2.025 eV. The position, quantum yield, and the spectral width of this peak are all in good agreement with previous reported values.[40,57,58]. The peak shifts to 2.023 eV in the 1L-ReS_2/1L-WS_2 heterostructure. The reduction of the optical bandgap of 2 meV can be attributed to the changes of both the bandgap and the exciton binding energy of WS_2 caused by the screening effect of ReS_2[40]. The peak further shifts to 2.021 eV in the 2L-ReS_2/1L-WS_2 heterostructure, which is consistent with the expected larger screening effect due to the doubled thickness. Furthermore, significant quenching of PL was observed in both heterostructures, suggesting efficient charge or energy transfer from WS_2 to ReS_2 on a time scale shorter than the exciton lifetime in WS_2. We moved the laser spot on each heterostructure region, and confirmed that the quenching factors of about 15 and 700 in the two regions are reproducible.

It is interesting to note that the spectrum of 2L-ReS_2/1L-WS_2 heterostructure has a shoulder at the low-energy side, which is absent in the other two regions. Since this shoulder is about 50 meV below the main peak, which is close to the trion binding energy of WS_2, we attribute this peak to trions, which is confirmed by the dependence of the PL spectrum on the excitation power (See Supplemental Material[59]). We note that this shoulder is also visible in the 1L-ReS_2/1L-WS_2 region, although it is less pronounced.

III. TIME-RESOLVED MEASUREMENTS

Charge carrier dynamics was studied by transient absorption measurements in the reflection geometry. In the experimental setup, a Ti:sapphire laser generates 100-fs pulses with a central wavelengths of about 780 - 790 nm, a spectral width of about 10 nm, and a repetition rate of 80 MHz. One part of this beam is sent to a nonlinear optical crystal to generate second harmonic pulses of about 390 - 395 nm. The rest of the beam is used to pump an optical parametric oscillator to produce near infrared pulse in the range of 1220 - 1280 nm, which second harmonic in the range of 610 - 640 nm is close to the optical bandgap of WS_2. The output of the Ti:sapphire can also be used directly in the experiment. In a certain experimental configuration, two of these pulses are used as the pump and probe, which are combined by a beamsplitter and are focused to the sample from normal direction through a microscope objective lens. The reflected probe beam is sent to a photodetector, which output is measured by a lock-in amplifier. The intensity of the pump beam is modulated by a mechanical chopper at about 3 KHz. With the configuration, the lock-in amplifier measured the differential reflection of the probe as the probe delay (defined as the arrival time of the probe pulse at the sample with respect to the pump pulse) is varied by changing the probe path length. The differential reflection is defined as $\Delta R/R_0 = (R - R_0)/R_0$, where R and R_0 are the probe reflectance with and without the presence of the pump beam, respectively.

We first studies photocarrier dynamics in individual 1L WS_2, 1L ReS_2, and 2L ReS_2 regions. For 1L-WS_2, a 3.18-eV pump pulse with an energy fluence of 3 μJ cm^{-2} was used to inject free carriers. Using an absorption coefficient of 7.5×10^7 m^{-1}[60], the estimated peak density of injected electron-hole pairs is about 3×10^{11} cm^{-2} . The differential reflection measured with a 2.01-eV probe pulse, which is near the optical bandgap of WS_2, is shown by the blue squares in Figure 2 for short (a) and long (b) time ranges, respectively. The rise of the signal can be fit by the integral of a Gaussian function with a full-width at half-maximum of 0.375 ps, as indicated by the curve in (a). This time is longer than the cross correlation of the pump and probe pulses of about 200 fs, which suggests that the injected free carriers produce maximum signal at the exciton resonance at a slightly delayed time.

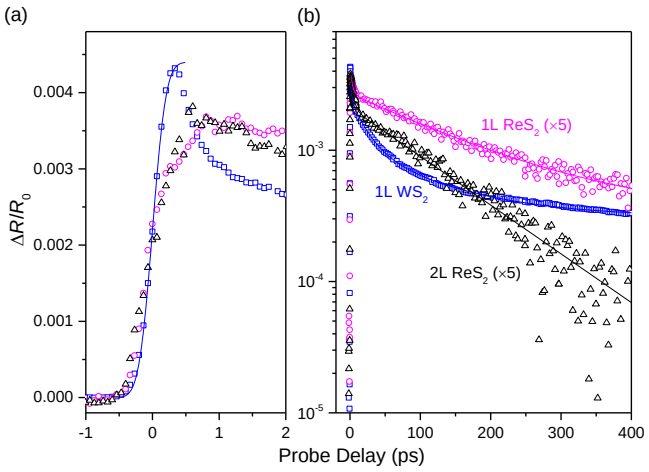

FIG. 2. Differential reflection of individual materials of 1L WS_2 (blue squares), 1L ReS_2 (magenta circles), and 2L ReS_2 (black triangles) over short (a) and long (b) time ranges. Photocarriers are injected by a 3.18-eV pump and detected by probes of 2.01 eV for WS_2 and 1.61 eV for both ReS_2 regions, respectively. The curves are fits (see text).

TABLE I. Summary of the time constants deduced from the exponential fits.

Sample	τ_1 (weight)	τ_2 (weight)	τ_3 (weight)	Background
1L WS_2	1.9 ± 0.3 ps (31 %)	22 ± 3 ps (39 %)	115 ± 30 ps (21 %)	9 %
1L ReS_2	3.6 ± 0.6 ps (33 %)	160 ± 20 ps (60 %)	– (0 %)	7 %
2L ReS_2	4.1 ± 0.4 ps (45 %)	117 ± 15 ps (55 %)	– (0 %)	0 %
1L-ReS_2/1L-WS_2	1.3 ± 0.2 ps (15 %)	330 ± 50 ps (7 %)	– (0 %)	78 %
2L ReS_2/1L-WS_2	1.0 ± 0.2 ps (50 %)	46 ± 5 ps (14 %)	– (0 %)	36 %

The decay of the signal can be fit by a tri-exponential function, $\Delta R/R_0(t) = A_1\exp(-t/\tau_1) + A_2\exp(-t/\tau_2) + A_3\exp(-t/\tau_3) + B$, as shown by the black curve in (b), with the three processes of time constants (and weights) of τ_1 of 1.9 ± 0.3 ps (31 %), τ_2 of 22 ± 3 ps (39 %), τ_3 of 115 ± 30 ps (21 %), and a background of 9 %. Based on previous studies, the τ_1 process can be related to formation of excitons from free carriers[61,62], which causes reduction of the signal. However, we note that the time constant observed from this sample is longer than previous studies[61,62]. The attribute the 22-ps process to exciton recombination, which is consistent with previously reported exciton lifetime in 1L WS_2[63]. The rest of the process, which accounts for about 30 % of the signal, could be attributed to effects of lattice heating by the laser pulse or defects. All the time constants are summarized in Table I for better comparison, along with those from the heterostructures.

The magenta and black symbols in Figure 2 show the signal from the 1L and 2L ReS_2 regions, respectively. For clarify, both signals have been multiplied by a factor of 5. In these measurements, the same pump photon energy (3.18 eV) and fluence (3 μJ cm^{-2}) were used, while the probe was tuned to 1.61 eV, which is about 0.1 eV above the optical bandgap of ReS_2. With an absorption coefficient of 3.5×10^7 m^{-1},[26] the pump injects a peak carrier density of 1.35×10^{11} and 2.7×10^{11} cm^{-2} in the 1L and 2L ReS_2 regions, respectively. From Figure 2(a), the signals show a slower rise, compared to WS_2, of about less than 1 ps. Since the pump photon energy is much larger than the bandgap of ReS_2, the rise could be attributed to energy relaxation of hot carriers from their injected states to the states that are probed. The decay of the signal in both regions can be fit by a biexponential function, $\Delta R/R_0(t) = A_1\exp(-t/\tau_1) + A_2\exp(-t/\tau_2) + B$. For the 1L, the two time constants are τ_1 = 3.6 ± 0.6 ps (33 %) and τ_2 = 160 ± 20 ps (60 %), with a background of 7 % (magenta curve). For the 2L, these parameters are τ_1 = 4.1 ± 0.4 ps (45 %) and τ_2 = 117 ± 15 ps (55 %), with almost no background (black curve). Both the magnitude and the time evolution of the signal from the two ReS_2 regions are similar, suggesting similar carrier dynamics in 1L and 2L ReS_2. The long time constants can be attributed to exciton lifetime in these samples.

With the information on carrier dynamics in the three individual materials, we next studied charge transfer between them. To probe potential hole transfer from ReS_2 to WS_2, we used the configuration shown in Figure 3(a). A 1.57-eV pump pulse selectively excites carriers in 1L or 2L ReS_2. Since the photon energy is smaller than its optical bandgap, the WS−2 layer is not excited. If the VBM of ReS_2 is lower than WS_2, as theoretically predicted, holes are expected to transfer to WS_2 to lower their potential energy. By using a probe tuned near the optical bandgap of WS_2, we monitor the appearance of these holes in WS_2 and time resolve their dynamics. Electrons are expected to reside in ReS_2, which has the lower CBM. The separation of the electrons and holes are expected to allow formation of spatially-indirect excitons with prolonged lifetime[64,65].

The differential reflection signals obtained with this configuration from the 1L-ReS_2/1L-WS_2 and 2L-ReS_2/1L-WS_2 het-

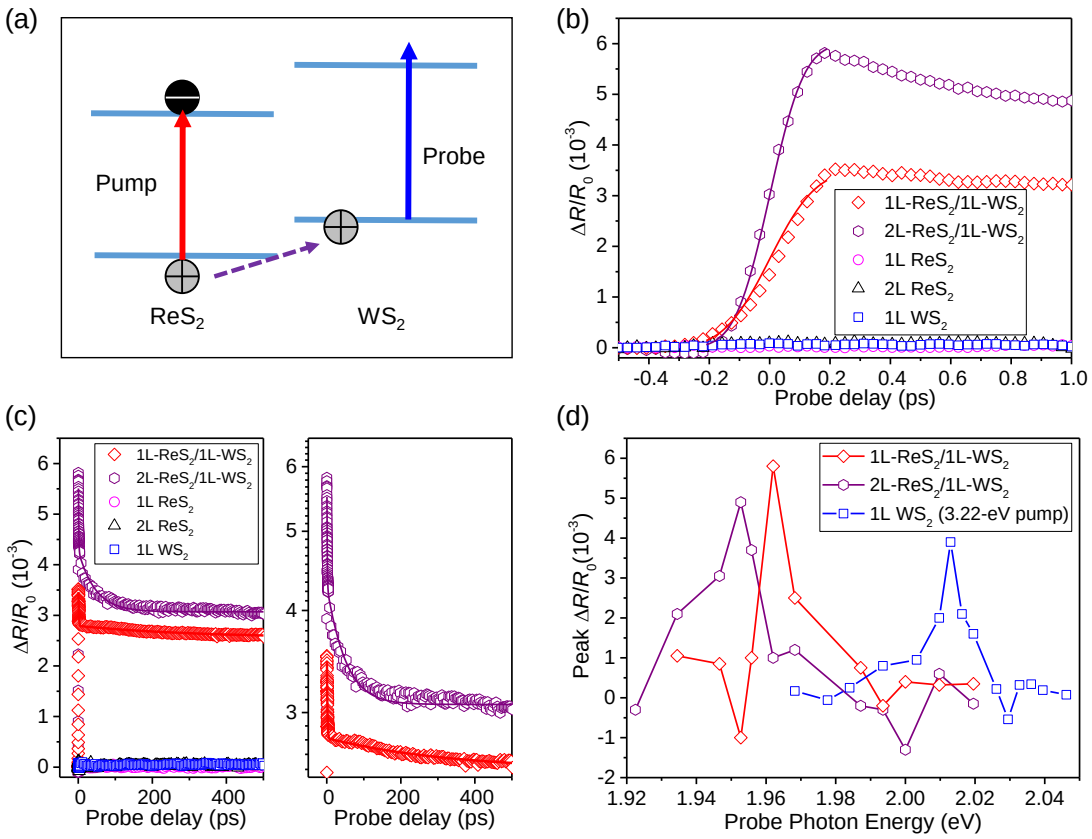

FIG. 3. (a) Schematics of the pump-probe configuration to study hole transfer from ReS_2 to WS_2. (b) Differential reflection signal obtained from the heterostructures of 1L-ReS_2/1L-WS_2 (red diamonds) and 2L-ReS_2/1L-WS_2 (purple hexagons) using the configuration shown in (a). Results of the same measurements on regions of 1L WS_2 (blue squares), 1L ReS_2 (magenta circles), and 2L ReS_2 (black triangles) are also shown for comparison. (c) Same as (b) but with a longer time range and with linear (left) and logarithmic scales. (d) Peak differential reflection signal as a function of the probe photon energy for the two heterostructures and the 1L WS_2

erostructures are shown by the red diamonds and purple hexagons in Figure 3(b) and (c) for short and long time ranges, respectively. In these measurements, the pump injects carrier densities of 4.1×10^{11} and 8.2×10^{11} cm^{-2} in 1L and 2L ReS_2, respectively. The probe photon energies used are 1.97 and 1.95 eV for 1L-Re_2/1L-WS_2 and 2L-ReS_2/1L-WS_2 heterostructures, respectively. The rather strong signal observed suggests the occurrence of hole transfer. We next studied the dependence of the signal magnitude on the probe photon energy for the two heterostructure samples. As shown in Figure 3(d), both heterostructures show pronounced resonant feature near the A-exciton of WS_2 that is consistent with PL peaks shown in Figure 1(c). For comparison, probe-photon-energy dependence of the 1L WS_2 sample was also plotted, which was obtained by using a pump pulse of 3.18 eV. These differential reflection spectra show that the signal indeed originates from the change of the excitonic resonance of WS_2, instead of from higher energy states in ReS_2. To further confirm the origin of the signal, we repeated the measurement on the three regions of the individual materials. No signal was observed, as shown by the magenta circles (1L ReS_2), black triangles (2L ReS_2), and blue squares (1L WS_2). This is expected, since for the 1L WS_2 region the pump does not inject carriers while for the ReS_2 regions the probe is far away from their optical bandgaps and thus has low probing efficiency.

Having established the hole transfer process, we now compare the two heterostructures. First, the red diamonds in Figure 3(b) show that the signal in 1L-ReS_2/1L-WS_2 rises to its peak rapidly. The red curve over the data represents the integral of a Gaussian function with a full-width at half-maximum of 280 fs, showing the ultrafast nature of the hole transfer process. Interestingly, for 2L-ReS_2/1L-WS_2, the rising time corresponds to a width of 220 fs, as shown as the purple circles and curve in Figure 3(b), which suggests that hole transfer from 2L ReS_2 to WS_2 is faster than from 1L ReS_2 to WS_2. If the two ReS_2 layers are decoupled with electrons localized in each layer, one would expect that the transfer from 2L to be slower with an additional transfer step between the two ReS_2 layers. Hence, we conclude the two ReS_2 layers are coupled and the holes are delocalized.

To analyze the carrier dynamics, we fit the decay process of the signal from the 1L-ReS_2/1L-WS_2 heterostructure with a bi-exponential function, $\Delta R/R_0(t) = A_1 \exp(-t/\tau_1) + A_2 \exp(-t/\tau_2) + B$. The results are plotted as the red curve over the data in Figure 3(c), with parameters of $A_1 = 0.5 \times 10^{-3}, A_2 = 0.24 \times 10^{-3}, B = 2.6 \times 10^{-3}, \tau_1 = 1.3 \pm 0.2$ ps, and $\tau_2 = 330 \pm 50$ ps. The fast process of picosecond has been similarly observed in TMD monolayers, and was attributed to exciton formation

of free electron-hole pairs[61,62], which lowers the effectiveness of carriers in changing the exciton resonance. Here, we assign this process to the formation of interlayer excitons between the transferred holes in WS_2 and the electrons in ReS_2. The most significant feature observed is the long-lived signal that accounts for a large portion (about 80 %) of the total signal. This suggest that indirect excitons formed after holes transfer have a very long lifetime, which is reasonable considering the spatial separation of electrons and holes This observation further confirms the type-II nature of the band alignment between 1L ReS_2 and 1L WS_2. We note that such long-lived and pronounced signal was not observed in the individual materials (see Figure 2). The intermediate τ_2 process accounts only for a few percent of the signal. This process could be due to various aspects of the dynamics of the indirect excitons following their formation, such as thermalization, energy relaxation, and multi-exciton annihilation. More studies are necessary for fully understanding this process. However, given that this process makes a minor (7%) contribution to the signal, the uncertainty of its nature does not influence the main conclusion of this study. The signal from 2L-ReS_2/1L-WS_2 (purple hexagons) is similar to 1L-ReS_2/1L-WS_2. By using the same bi-exponential function (purple curve over the data), we find the parameter of $A_1 = 4.4 \times 10^{-3}, A_2 = 1.2 \times 10^{-3}, B = 3.1 \times 10^{-3}, \tau_1 = 1.0 \pm 0.2$ ps, and $\tau_2 = 46 \pm 5$ ps. Similarly, indirect excitons have a very long lifetime. We note that unlike the 1L WS_2 sample, no effect from lattice heating was observed here, due to the dominate signal from indirect excitons.

IV. CONCLUSION

We have observed interlayer charge transfer in heterostructures of 1L-ReS_2/1L-WS_2 and 2L-ReS_2/1L-WS_2 by femtosecond transient absorption measurements. In the former heterostructure, holes injected in ReS_2 transfer to WS_2 on an ultrafast time scale, which is encouraging news for incorporating ReS_2 to the material library for fabricating van der Waals heterostructure. The hole transfer from 2L ReS_2 to WS_2 was found to be even faster. If the holes in 2L ReS_2 were localized in each layer, the transfer would require an additional step of interlayer transfer within ReS_2 and thus would have been slower. Hence, this observation is evidence that the holes are delocalized, illustrating the strong interlayer coupling in ReS_2. The difference in the charge transfer time could be attributed to the different bandstructures in 1L and 2L ReS_2. These results show that the band alignment of both heterostructures is type II, which is consistent with theoretical predictions.

V. ACKNOWLEDGMENT

We are grateful for the financial support of the National Key R&D Program of China (2016 YFA0202302), the National Natural Science Foundation of China (61527817, 61875236), and National Science Foundation of USA (DMR-1505852).

* yshwang@bjtu.edu.cn
† huizhao@ku.edu

[1] K. S. Novoselov, A. Mishchenko, A. Carvalho, and A. H. C. Neto, Science **353**, 461 (2016).
[2] G. Wang, A. Chernikov, M. M. Glazov, T. F. Heinz, X. Marie, T. Amand, and B. Urbaszek, Rev. Mod. Phys. **90**, 021001 (2018).
[3] S. Manzeli, D. Ovchinnikov, D. Pasquier, O. V. Yazyev, and A. Kis, Nature Reviews Materials **2**, 17033 (2017).
[4] Z. Lin, A. McCreary, N. Briggs, S. Subramanian, K. H. Zhang, Y. F. Sun, X. F. Li, N. J. Borys, H. T. Yuan, S. K. Fullerton-Shirey, A. Chernikov, H. Zhao, S. McDonnell, A. M. Lindenberg, K. Xiao, B. J. LeRoy, M. Drndic, J. C. M. Hwang, J. Park, M. Chhowalla, R. E. Schaak, A. Javey, M. C. Hersam, J. Robinson, and M. Terrones, 2D Mater. **3**, 042001 (2016).
[5] S. Tongay, H. Sahin, C. Ko, A. Luce, W. Fan, K. Liu, J. Zhou, Y.-S. Huang, C.-H. Ho, J. Yan, D. F. Ogletree, S. Aloni, J. Ji, S. Li, J. Li, F. M. Peeters, and J. Wu, Nat. Commun. **5**, 3252 (2014).
[6] S. P. Kelty, A. F. Ruppert, R. R. Chianelli, J. Ren, and M. H. Whangbo, J. Am. Chem. Soc. **116**, 7857 (1994).
[7] H. H. Murray, S. P. Kelty, R. R. Chianelli, and C. S. Day, Inorg. Chem. **33**, 4418 (1994).
[8] C. H. Ho, Y. S. Huang, K. K. Tiong, and P. C. Liao, Phys. Rev. B **58**, 16130 (1998).
[9] Q. Cui, J. He, M. Z. Bellus, M. Mirzokarimov, T. Hofmann, H.-Y. Chiu, M. Antonik, D. He, Y. Wang, and H. Zhao, Small **11**, 5565 (2015).
[10] O. B. Aslan, D. A. Chenet, A. M. van der Zande, J. C. Hone, and T. F. Heinz, ACS Photon. **3**, 96 (2016).
[11] Q. Cui, R. A. Muniz, J. E. Sipe, and H. Zhao, Phys. Rev. B **95**, 165406 (2017).
[12] S. S. Zhang, N. N. Mao, N. Zhang, J. X. Wu, L. M. Tong, and J. Zhang, ACS Nano **11**, 10366 (2017).
[13] C. H. Ho, Y. S. Huang, K. K. Tiong, and P. C. Liao, J. Phys. - Condens. Mat. **11**, 5367 (1999).
[14] Y. C. Lin, H. P. Komsa, C. H. Yeh, T. Bjorkman, Z. Y. Liang, C. H. Ho, Y. S. Huang, P. W. Chiu, A. V. Krasheninnikov, and K. Suenaga, ACS Nano **9**, 11249 (2015).
[15] K. Friemelt, M. C. Luxsteiner, and E. Bucher, J. Appl. Phys. **74**, 5266 (1993).
[16] F. F. Cui, C. Wang, X. B. Li, G. Wang, K. Q. Liu, Z. Yang, Q. L. Feng, X. Liang, Z. Y. Zhang, S. Z. Liu, Z. B. Lei, Z. H. Liu, H. Xu, and J. Zhang, Adv. Mater. **28**, 5019 (2016).

[17] X. B. Li, F. F. Cui, Q. L. Feng, G. Wang, X. S. Xu, J. X. Wu, N. N. Mao, X. Liang, Z. Y. Zhang, J. Zhang, and H. Xu, Nanoscale **8**, 18956 (2016).
[18] K. Keyshar, Y. J. Gong, G. L. Ye, G. Brunetto, W. Zhou, D. P. Cole, K. Hackenberg, Y. M. He, L. Machado, M. Kabbani, A. H. C. Hart, B. Li, D. S. Galvao, A. George, R. Vajtai, C. S. Tiwary, and P. M. Ajayan, Adv. Mater. **27**, 4640 (2015).
[19] K. D. Wu, B. Chen, S. J. Yang, G. Wang, W. Kong, H. Cai, T. Aoki, E. Soignard, X. Marie, A. Yano, A. Suslu, B. Urbaszek, and S. Tongay, Nano Lett. **16**, 5888 (2016).
[20] J. Shim, A. Oh, D. H. Kang, S. Oh, S. K. Jang, J. Jeon, M. H. Jeon, M. Kim, C. Choi, J. Lee, S. Lee, G. Y. Yeom, Y. J. Song, and J. H. Park, Adv. Mater. **28**, 6985 (2016).
[21] A. Dathbun, Y. Kim, S. Kim, Y. Yoo, M. S. Kang, C. Lee, and J. H. Cho, Nano Lett. **17**, 2999 (2017).
[22] E. Zhang, Y. B. Jin, X. Yuan, W. Y. Wang, C. Zhang, L. Tang, S. S. Liu, P. Zhou, W. D. Hu, and F. X. Xiu, Adv. Funct. Mater. **25**, 4076 (2015).
[23] E. F. Liu, M. S. Long, J. W. Zeng, W. Luo, Y. J. Wang, Y. M. Pan, W. Zhou, B. G. Wang, W. D. Hu, Z. H. Ni, Y. M. You, X. A. Zhang, S. Q. Qin, Y. Shi, K. Watanabe, T. Taniguchi, H. T. Yuan, H. Y. Hwang, Y. Cui, F. Miao, and D. Y. Xing, Adv. Funct. Mater. **26**, 1938 (2016).
[24] C. M. Corbett, C. McClellan, A. Rai, S. S. Sonde, E. Tutuc, and S. K. Banerjee, ACS Nano **9**, 363 (2015).
[25] F. C. Liu, S. J. Zheng, X. X. He, A. Chaturvedi, J. F. He, W. L. Chow, T. R. Mion, X. L. Wang, J. D. Zhou, Q. D. Fu, H. J. Fan, B. K. Tay, L. Song, R. H. He, C. Kloc, P. M. Ajayan, and Z. Liu, Adv. Funct. Mater. **26**, 1169 (2016).
[26] K. Friemelt, L. Kulikova, L. Kulyuk, A. Siminel, E. Arushanov, C. Kloc, and E. Bucher, J. Appl. Phys. **79**, 9268 (1996).
[27] C. H. Ho, P. C. Liao, Y. S. Huang, and K. K. Tiong, Phys. Rev. B **55**, 15608 (1997).
[28] C. H. Ho, P. C. Liao, Y. S. Huang, and K. K. Tiong, Solid State Commun. **103**, 19 (1997).
[29] C. H. Ho, Y. S. Huang, J. L. Chen, T. E. Dann, and K. K. Tiong, Phys. Rev. B **60**, 15766 (1999).
[30] I. Gutierrez-Lezama, B. A. Reddy, N. Ubrig, and A. F. Morpurgo, 2D Mater. **3**, 045016 (2016).
[31] N. B. Mohamed, K. Shinokita, X. F. Wang, H. E. Lim, D. Z. Tan, Y. Miyauchi, and K. Matsuda, Appl. Phys. Lett. **113**, 121112 (2018).
[32] M. Gehlmann, I. Aguilera, G. Bihlmayer, S. Nemsak, P. Nagler, P. Gospodaric, G. Zamborlini, M. Eschbach, V. Feyer, F. Kronast, E. Mlynczak, T. Korn, L. Plucinski, C. Schuller, S. Blugel, and C. M. Schneider, Nano Lett. **17**, 5187 (2017).
[33] Q. Zhang, S. J. Tan, R. G. Mendes, Z. T. Sun, Y. T. Chen, X. Kong, Y. H. Xue, M. H. Rummeli, X. J. Wu, S. L. Chen, and L. Fu, Adv. Mater. **28**, 2616 (2016).
[34] R. He, J. A. Yan, Z. Y. Yin, Z. P. Ye, G. H. Ye, J. Cheng, J. Li, and C. H. Lui, Nano Lett. **16**, 1404 (2016).
[35] E. Lorchat, G. Froehlicher, and S. Berciaud, ACS Nano **10**, 2752 (2016).
[36] X. F. Qiao, J. B. Wu, L. W. Zhou, J. S. Qiao, W. Shi, T. Chen, X. Zhang, J. Zhang, W. Ji, and P. H. Tan, Nanoscale **8**, 8324 (2016).
[37] D. Ovchinnikov, F. Gargiulo, A. Allain, D. J. Pasquier, D. Dumcenco, C. H. Ho, O. V. Yazyev, and A. Kis, Nat. Commun. **7**, 12391 (2016).
[38] X. Hong, J. Kim, S. F. Shi, Y. Zhang, C. Jin, Y. Sun, S. Tongay, J. Wu, Y. Zhang, and F. Wang, Nat. Nanotechnol. **9**, 682 (2014).
[39] F. Ceballos, M. Z. Bellus, H. Y. Chiu, and H. Zhao, ACS Nano **8**, 12717 (2014).
[40] F. Ceballos, M. Z. Bellus, H. Y. Chiu, and H. Zhao, Nanoscale **7**, 17523 (2015).
[41] B. Peng, G. Yu, X. Liu, B. Liu, X. Liang, L. Bi, L. Deng, T. C. Sum, and K. P. Loh, 2D Mater. **3**, 025020 (2016).
[42] H. M. Zhu, J. Wang, Z. Z. Gong, Y. D. Kim, J. Hone, and X. Y. Zhu, Nano Lett. **17**, 3591 (2017).
[43] L. Yuan, T. F. Chung, A. Kuc, Y. Wan, Y. Xu, Y. P. Chen, T. Heine, and L. B. Huang, Sci. Adv. **4**, e1700324 (2018).
[44] X. W. Wen, H. L. Chen, T. M. Wu, Z. H. Yu, Q. R. Yang, J. W. Deng, Z. T. Liu, X. Guo, J. X. Guan, X. Zhang, Y. J. Gong, J. T. Yuan, Z. H. Zhang, C. Y. Yi, X. F. Guo, P. M. Ajayan, W. Zhuang, Z. R. Liu, J. Lou, and J. R. Zheng, Nat. Commun. **9**, 1859 (2018).
[45] M. Z. Bellus, M. Li, S. Lane, F. Ceballos, Q. Cui, X. C. Zeng, and H. Zhao, Nanoscale Horiz. **2**, 31 (2016).
[46] C. Park, N. T. Duong, S. Bang, D. A. Nguyen, H. M. Oh, and M. S. Jeong, Nanoscale **10**, 20306 (2018).
[47] J. Shim, S. Oh, D. H. Kang, S. H. Jo, M. H. Ali, W. Y. Choi, K. Heo, J. Jeon, S. Lee, M. Kim, Y. J. Song, and J. H. Park, Nat. Commun. **7**, 13413 (2016).
[48] T. Zhang, B. Jiang, Z. Xu, R. G. Mendes, Y. Xiao, L. F. Chen, L. W. Fang, T. Gemming, S. L. Chen, M. H. Rummeli, and L. Fu, Nat. Commun. **7**, 13911 (2016).
[49] B. Kang, Y. Kim, W. J. Yoo, and C. Lee, Small **14**, 1802593 (2018).
[50] V. O. Özcelik, J. G. Azadani, C. Yang, S. J. Koester, and T. Low, Phys. Rev. B **94**, 035125 (2016).
[51] C. Ruppert, O. B. Aslan, and T. F. Heinz, Nano Lett. **14**, 6231 (2014).
[52] F. Ceballos, P. Zereshki, and H. Zhao, Phys. Rev. Mater. **1**, 044001 (2017).
[53] P. Zereshki, Y. Q. Wei, F. Ceballos, M. Z. Bellus, S. D. Lane, S. D. Pan, R. Long, and H. Zhao, Nanoscale **10**, 11307 (2018).
[54] P. Zereshki, Y. Wei, R. Long, and H. Zhao, J. Phys. Chem. Lett. **9**, 5970 (2018).
[55] J. Kang, S. Tongay, J. Zhou, J. B. Li, and J. Q. Wu, Appl. Phys. Lett. **102**, 012111 (2013).
[56] M. Li, M. Z. Bellus, J. Dai, L. Ma, X. L. Li, H. Zhao, and X. C. Zeng, Nanotechnology **29**, 335203 (2018).
[57] N. Peimyoo, W. Yang, J. Shang, X. Shen, Y. Wang, and T. Yu, ACS Nano **8**, 11320 (2014).
[58] Z. Ye, T. Cao, K. O'Brien, H. Zhu, X. Yin, Y. Wang, S. G. Louie, and X. Zhang, Nature **513**, 214 (2014).
[59] See Supplemental Material at [URL will be inserted by publisher] for more data on identification of the trion peak.
[60] H.-L. Liu, C.-C. Shen, S.-H. Su, C.-L. Hsu, M.-Y. Li, and L.-J. Li, Appl. Phys. Lett. **105**, 201905 (2014).
[61] F. Ceballos, Q. Cui, M. Z. Bellus, and H. Zhao, Nanoscale **8**, 11681 (2016).
[62] P. Steinleitner, P. Merkl, P. Nagler, J. Mornhinweg, C. Schuller, T. Korn, A. Chernikov, and R. Huber, Nano Lett. **17**, 1455 (2017).
[63] C. Mai, Y. G. Semenov, A. Barrette, Y. F. Yu, Z. H. Jin, L. Y. Cao, K. W. Kim, and K. Gundogdu, Phys. Rev. B **90**, 041414 (2014).
[64] P. Rivera, J. R. Schaibley, A. M. Jones, J. S. Ross, S. Wu, G. Aivazian, P. Klement, K. Seyler, G. Clark, N. J. Ghimire, J. Yan, D. G. Mandrus, W. Yao, and X. Xu, Nat. Commun. **6**, 6242 (2015).
[65] P. Nagler, G. Plechinger, M. V. Ballottin, A. Mitioglu, S. Meier, N. Paradiso, C. Strunk, A. Chernikov, P. C. M. Christianen, C. Schuller, and T. Korn, 2D Mater. **4**, 025112 (2017).